Cell Metabolism
Article

Mitochondrial Ca^{2+} Uptake Induces Cyclic AMP Generation in the Matrix and Modulates Organelle ATP Levels

Giulietta Di Benedetto,[1,2,*] Elisa Scalzotto,[2,4] Marco Mongillo,[1,2,3] and Tullio Pozzan[1,2,3]
[1]Institute of Neuroscience, Italian National Research Council (CNR), Viale G. Colombo 3, 35121 Padova, Italy
[2]Venetian Institute of Molecular Medicine (VIMM), Via Orus 2, 35129 Padova, Italy
[3]Department of Biomedical Sciences, University of Padova, Viale G. Colombo 3, 35121 Padova, Italy
[4]Present address: Department of Nephrology Dialysis & Transplantation, International Renal Research Institute Vicenza (IRRIV), St. Bortolo Hospital, 36100 Vicenza, Italy
*Correspondence: giulietta.dibenedetto@cnr.it
http://dx.doi.org/10.1016/j.cmet.2013.05.003

SUMMARY

While the role of mitochondrial Ca^{2+} homeostasis in cell pathophysiology is widely accepted, the possibility that cAMP regulates mitochondrial functions has only recently received experimental support. The site of cAMP production, its targets, and its functions in the organelles remain uncertain. Using a variety of genetic/pharmacological tools, we here demonstrate that the mitochondrial inner membrane is impermeable to cytosolic cAMP, while an autonomous cAMP signaling toolkit is expressed in the matrix. We demonstrate that rises in matrix Ca^{2+} powerfully stimulate cAMP increases within mitochondria and that matrix cAMP levels regulate their ATP synthesizing efficiency. In cardiomyocyte cultures, mitochondrial cAMP can be increased by treatments that augment the frequency and amplitude of Ca^{2+} oscillations within the cytosol and organelles, revealing that mitochondria can integrate an oscillatory Ca^{2+} signal to increase cAMP in their matrix. The present data reveal the existence, within mitochondria, of a hitherto unknown crosstalk between Ca^{2+} and cAMP.

INTRODUCTION

The discovery of the major role played by mitochondria in Ca^{2+} signaling, the understanding of their central role in cell death, and the increasing awareness of the linkage between mitochondrial dysfunctions and major human diseases have all led to a renewed interest in these organelles. While the role of mitochondria in Ca^{2+} homeostasis has been extensively investigated, the other major second messenger, cAMP, has remained for many years at the periphery of the mitochondrial saga, and its role in mitochondrial pathophysiology was hardly considered until recently. In the last years, however, the role of cAMP in modulating mitochondrial functions has been re-evaluated. DiPilato and coworkers, using a fluorescent cAMP sensor in live cells, concluded that cAMP produced in the cytoplasm diffuses rapidly into the mitochondrial matrix (DiPilato et al., 2004); Acin-Perez and coworkers, on the contrary, argued that the inner mitochondrial membrane is impermeable to cAMP and suggested that the organelles are endowed with a cAMP signaling cascade wholly contained in their matrix (Acin-Perez et al., 2009). They suggested that cAMP is generated inside the matrix by a soluble form of adenylate cyclase (sAC) (Chen et al., 2000) in response to bicarbonate; in turn, cAMP activates a mitochondrial isoform of protein kinase A, PKA, leading to the phosphorylation and activation of the respiratory chain (Acin-Perez et al., 2009, 2011a). In addition, phosphoproteomic studies revealed the presence of a number of mitochondrial phosphoproteins (Balaban, 2010; Boja et al., 2009; Hopper et al., 2006), some of which are potential targets of PKA (Zhao et al., 2011). On the other hand, whereas it is now firmly established that the outer (and possibly also the inner) mitochondrial membrane is enriched in PKA anchoring proteins (Alto et al., 2002; Carlucci et al., 2008; Chen et al., 1997; Huang et al., 1999; Liu et al., 2003; Means et al., 2011) and that phosphorylation of outer membrane proteins by cytosolic PKA has important functional effects in the organelles (Danial et al., 2003; Gomes et al., 2011; Harada et al., 1999), no recognizable mitochondrial signal sequence is present either in the R or C PKA subunits.

Here we show that changes in cAMP occur inside mitochondria of intact cells and that sAC is indeed the local cAMP source, while no diffusion of cytosolic cAMP takes place in healthy organelles. We also demonstrate that cAMP is generated in the matrix not only in response to changes in HCO_3^- concentration, but also upon increases in matrix Ca^{2+} levels. In cardiac myocytes in culture, an increase in the frequency and amplitude of Ca^{2+} oscillations, within cytoplasm and mitochondria, elicited by β-adrenergic stimulation or by the transmembrane AC (tmACs) activator forskolin, results in a rapid reversible increase of matrix cAMP level. Finally, we provide evidence that cAMP in the matrix contributes to the regulation of mitochondrial ATP production. The pharmacological sensitivity of the cAMP-dependent increase in mitochondrial ATP only in part overlaps that of cytosolic PKA.

RESULTS

Sensors for Monitoring Mitochondrial cAMP

Generation of FRET-Based cAMP Sensors Selectively Targeted to the Mitochondrial Matrix

DiPilato et al. suggested that cytosolic cAMP increases are paralleled by similar changes within the mitochondrial matrix

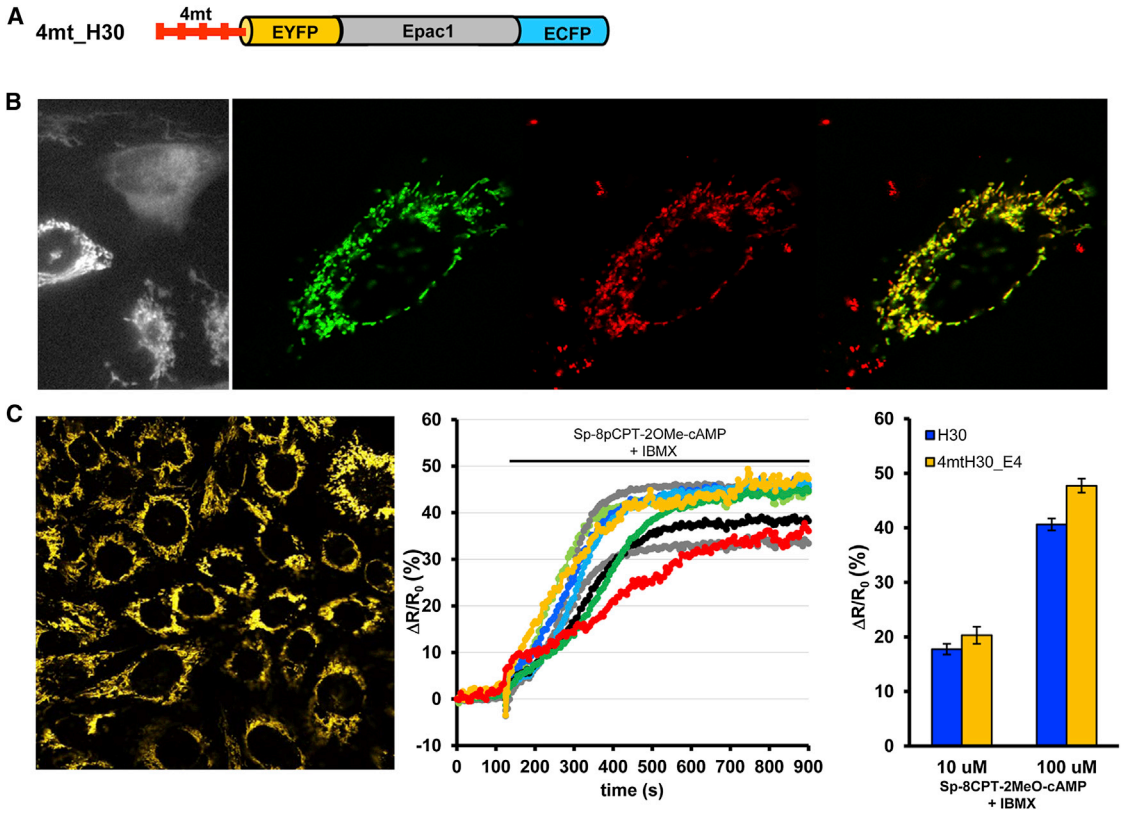

Figure 1. Mitochondrial Localization of the cAMP Sensor and FRET Changes Caused by a Membrane-Permeable cAMP Analog

(A) Schematic representation of the matrix-targeted cAMP sensor 4mtH30. Four copies of the human COXVIII targeting sequence have been fused to the N terminus of H30, which contains, between ECFP and EYFP, the whole Epac1 protein, rendered catalytically inactive and deprived of the membrane-targeting DEP domain.

(B) Left panel: Representative epifluorescence images of HeLa cells transiently expressing 4mtH30, 24 hr after transfection. The cAMP probe localizes preferentially in rod-like elongated structures, though in some cells (see, for example, the upper cell) a significant mislocalization in the cytosol is evident. The sensors' localization, however, becomes exclusively mitochondrial in almost all cells 48 hr after transfection. Right panel: Representative images of a HeLa cell co-transfected with the cAMP sensor 4mtH30 (green) and the mitochondrial fluorescent protein mtRFP (red). The colocalization of 4mtH30 with mtRFP indicates a very good overlapping between the two signals (yellow). Similar results were obtained in CHO cells.

(C) Left panel: Representative confocal image of the 4mtH30_E4 stable cell line indicating that these cells correctly express 4mtH30 within mitochondria, without any appreciable cytosolic mistargeting. Middle panel: Representative kinetics of $\Delta R/R_0$ recorded in several 4mtH30_E4 cells challenged, in the presence of IBMX (100 μM), with Sp-8-pCPT-2′-O-Me-cAMPS (100 μM), a highly membrane-permeable cAMP analog that selectively activates Epac. Right panel: Blue columns: average percentage $\Delta R/R_0$ increases (mean ± SEM) observed upon addition of 10 or 100 μM Sp-8-pCPT-2′-O-Me-cAMPS, in the presence of 100 μM IBMX, to cells transiently expressing cytosolic H30. Number of cells (n) = 10 for each condition. Yellow columns: as above, but in 4mtH30_E4, i.e., the cell line stably expressing the mitochondrial targeted probe, n = 12. In these and the following experiments the average values were obtained from at least three independent experiments and the error bars in the columns represent SEM.

(DiPilato et al., 2004). Using the very same sensor, we observed that the probe is extensively missorted to the cytosol with only a marginal accumulation in mitochondria (not shown). We thus generated new cAMP sensors with improved mitochondrial targeting (Filippin et al., 2005) by fusing repetitive (two or four copies) targeting sequences from subunit VIII of the human cytochrome oxidase (COX) at the N terminus of either the cAMP sensor Epac1-camp (Nikolaev et al., 2004) (not shown) or CFP-Epac(δDEP-CD)-YFP, named H30 (Ponsioen et al., 2004) (Figure 1A). Out of the different constructs generated, we selected 4mtH30, as it displays the largest dynamic changes in response to cAMP variations. When cells transiently expressing 4mtH30 were analyzed 24 hr from transfection, the probe was in some cells partially missorted to the cytosol (Figure 1B, left panel), but it was almost exclusively mitochondrial after 48 hr (Figure 1B, right panel). The selective localization in the matrix was verified as described in Supplemental Information (see also Giacomello et al., 2010). A CHO cell line stably expressing the 4mtH30 probe was generated. Confocal images of the 4mtH30_E4 stable line (Figure 1C, left) indicate that 4mtH30 is correctly localized in mitochondria, without any appreciable cytosolic mistargeting.

Changes in cAMP levels were assessed by measuring the 480/540 nm emission ratio upon excitation at 430 nm and presented as $\Delta R/R_0$, where R is the ratio at time t, R_0 is the ratio at time 0, and $\Delta R = R - R_0$. Typical kinetics of $\Delta R/R_0$ in several 4mtH30_E4 cells challenged with Sp-8-pCPT-2′-O-Me-cAMPS, a highly membrane-permeable Epac selective cAMP analog, are presented in Figure 1C (middle panel). The right panel of Figure 1C summarizes the maximal $\Delta R/R_0$ changes in cells expressing 4mtH30 or cytosolic H30, induced by 10 μM or

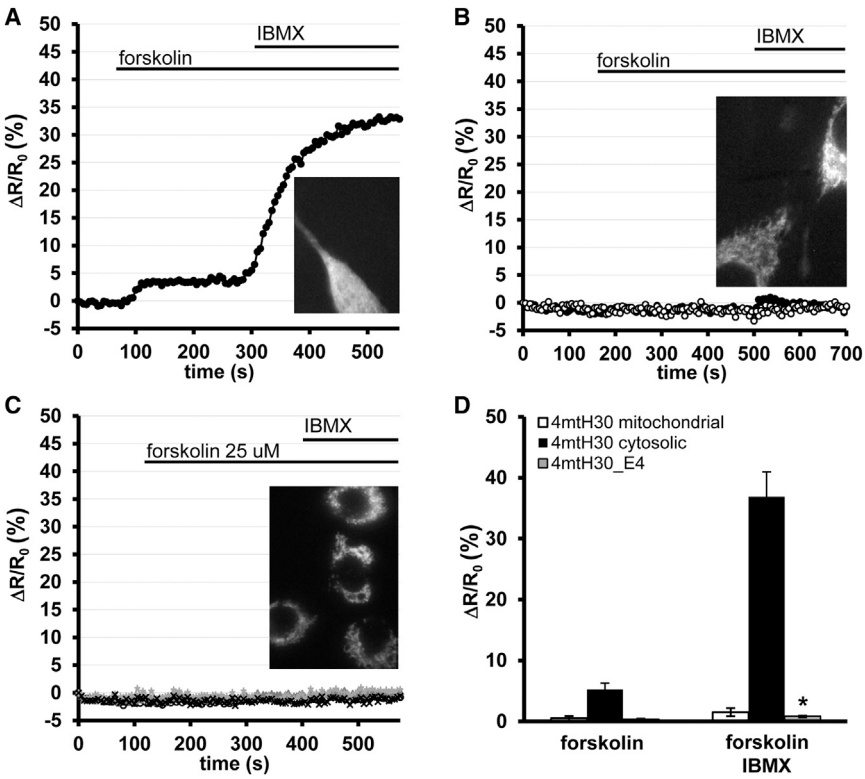

Figure 2. Mitochondria Are Impermeable to Cytosolic Changes of cAMP

(A–D) Representative kinetics of $\Delta R/R_0$ changes upon addition of forskolin (25 μM) followed by IBMX (100 μM) recorded in: (A) a representative HeLa cell transiently transfected with 4mtH30 and expressing the sensor mistargeted to the cytosol, (B) two representative HeLa cells transiently expressing 4mtH30 in the mitochondrial matrix, and (C) four stably expressing 4mtH30_E4 cells. In the insets of (A)–(C), the fluorescence pattern of the probe distribution in the analyzed cells is presented. The average $\Delta R/R_0$ increases (mean ± SEM) caused by forskolin and forskolin + IBMX are presented in (D) in cells transiently expressing cytosolic 4mtH30 (n = 8), 4mtH30 (n = 7), and in the stable line 4mtH30_E4 (n = 20). IBMX caused a very small but significant rise of $\Delta R/R_0$ in the mitochondrial matrix of the stable line 4mtH30_E4, whether added alone (not shown) or in the presence of forskolin: *p = 0.025, two-tailed paired t test.

100 μM Sp-8-pCPT-2′-O-Me-cAMPS in the presence of the PDE inhibitor IBMX (3-isobutyl-1-methylxanthine). The 4mtH30 sensor in the matrix environment displays a maximum ΔR comparable to that displayed by cytosolic H30.

cAMP Changes within the Mitochondrial Matrix

cAMP Generated in the Cytosol Does Not Diffuse into the Mitochondrial Matrix

We first tested whether cAMP generated in the cytosol could enter the mitochondrial matrix. To this end, the classical tmACs activator forskolin was used to induce a rise in cAMP. Figure 2A shows a representative kinetic of $\Delta R/R_0$ changes in the cytosol, recorded in a HeLa cell with a significant fraction of 4mtH30 mistargeted in the cytosol. Similar results were obtained in cells transiently expressing cytosolic H30 (not shown). In both cases, 25 μM forskolin caused a clear rise in cAMP. On the contrary, in HeLa cells transfected with 4mtH30 in which the probe is correctly targeted to the mitochondria (Figure 2B), or in cells stably expressing 4mtH30 (4mtH30_E4) (Figure 2C), forskolin had no effect on $\Delta R/R_0$. The generic PDE inhibitor IBMX, added after forskolin, caused a dramatic further increase in cytosolic cAMP (Figure 2A) and a very small but significant increase in mitochondrial cAMP (Figure 2B and 2C). This latter result suggests that mitochondrial cAMP could be modulated by endogenous PDEs. The average changes in cytosolic and matrix cAMP upon addition of forskolin and IBMX are summarized in Figure 2D.

Ca^{2+} Increases Induce cAMP Rises in the Mitochondrial Matrix

Indirect evidence has been provided indicating that sAC, in addition to its cytosolic location, is also present in the mitochondrial matrix (Acin-Perez et al., 2009). The enzymatic activity of sAC is increased by HCO_3^- and Ca^{2+} in a synergistic or additive way (Jaiswal and Conti, 2003; Litvin et al., 2003; Steegborn et al., 2005a, 2005b). To test whether Ca^{2+} could modulate mitochondrial cAMP, cells were incubated in a Ca^{2+}-free medium and challenged first with the IP_3-generating agonist ATP in combination with *tert*-Butylhydroquinone (TBHQ), an inhibitor of the sarco-endoplasmic reticulum Ca^{2+} ATPase. This protocol induces the release of Ca^{2+} from the ER; $CaCl_2$ was then reintroduced into the medium. Under these conditions capacitative Ca^{2+} influx (CCE) is maximally activated (Parekh and Putney, 2005), resulting in a large and sustained increase in Ca^{2+} entry from the medium (Putney, 2009) (Figure S1A).

We next measured, using the same protocol, the dynamics of mitochondrial cAMP (mt-cAMP) in the 4mtH30_E4 cell line. Addition of extracellular ATP + TBHQ caused a transient, small, and often unappreciable increase in mt-cAMP (Figure 3A). Ca^{2+} readdition caused, in almost all cells, a slow but marked increase in mt-cAMP; the final HCO_3^- administration induced a further increase (Figure 3A). The small mt-cAMP response to ATP + TBHQ increased in the presence of CGP 37157, a potent inhibitor of the mitochondrial Na^+/Ca^{2+} exchanger (mNCX) (Figures S1B–S1D).

It has been demonstrated that overexpression of the mitochondrial Ca^{2+} uniporter (MCU) (Baughman et al., 2011; De Stefani et al., 2011) results in a substantial increase in the amplitude of mitochondrial Ca^{2+} accumulation both in response to Ca^{2+} release from stores and to Ca^{2+} influx from the medium (De Stefani et al., 2011). We thus repeated the experiment in 4mtH30_E4 cells transiently expressing a mCherry-tagged version of MCU. In this case the amplitudes of the mt-cAMP rise in response to ATP (Figure 3B) or CCE (Figure 3C) were substantially increased. The percentage of ATP-responsive cells in the 4mtH30_E4 coexpressing MCU increased from 41% to 75%. The average mt-cAMP increases caused by ATP + TBHQ followed by Ca^{2+} in

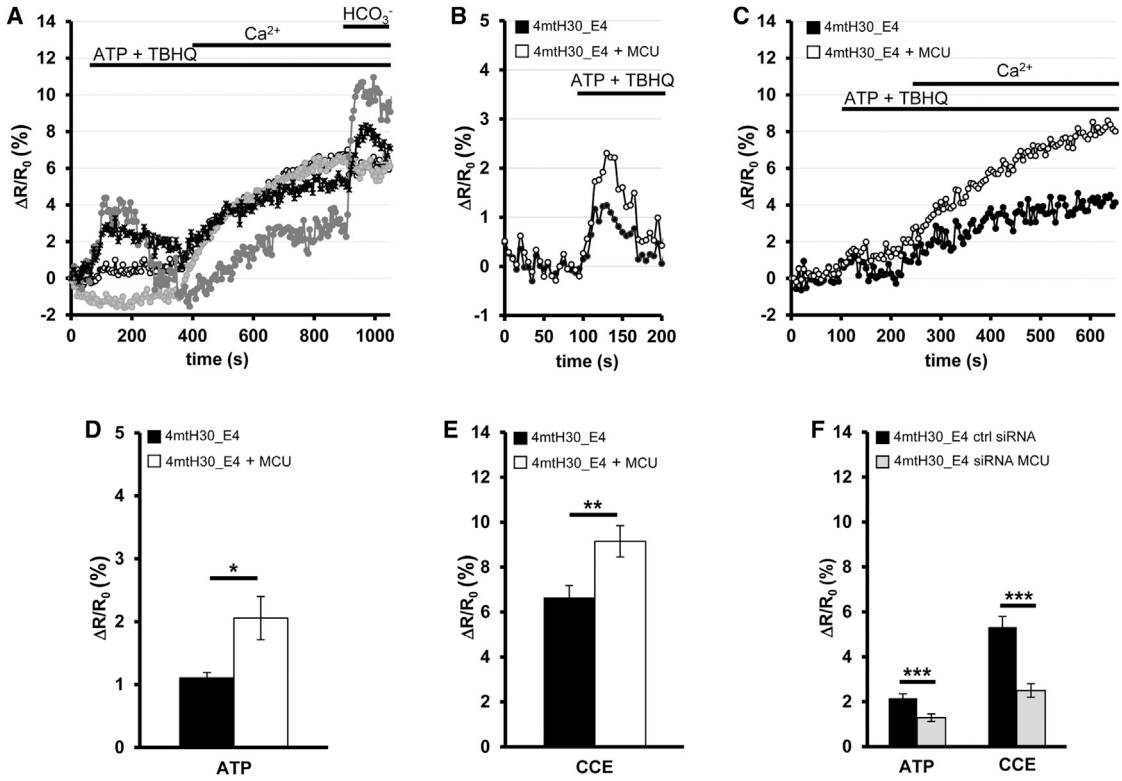

Figure 3. Ca^{2+} Increases in the Mitochondrial Matrix Are Paralleled by Mitochondrial cAMP Rises

(A) Representative kinetics of $\Delta R/R_0$ changes recorded in typical 4mtH30_E4 cells, stimulated, in sequence, with ATP (50 μM) + TBHQ (30 μM), $CaCl_2$ (2 mM), and $NaHCO_3$ (50 mM). The cells were first incubated in Ca^{2+}-free medium (containing 100 μM EGTA), and the perfusion buffer was changed, where indicated, with the same medium supplemented with ATP and TBHQ, followed by medium containing $CaCl_2$ +TBHQ and $CaCl_2$+ TBHQ and HCO_3^-.

(B and C) Representative kinetics of $\Delta R/R_0$ changes recorded in typical 4mtH30_E4 cells overexpressing a mCherry-tagged version of MCU, stimulated with ATP (50 μM) + TBHQ (30 μM) (B) followed by $CaCl_2$ (2 mM) (C).

(D and E) Average amplitude of the cAMP responses to ATP and CCE (mean ± SEM), without (n = 15, *p = 0.019) and with MCU overexpression (n = 15, **p = 0.009).

(F) Average amplitude of the cAMP responses to ATP and CCE (mean ± SEM), in 4mtH30_E4 cells treated with a scrambled siRNA (n = 23) or with a siRNA for MCU (n = 31); ***p = 0.001 for ATP and ***p = 2.6×10^{-6} for CCE. See also Figure S1.

controls and MCU-overexpressing cells are summarized in Figures 3D and 3E. On the contrary, when performing RNA silencing of MCU, both the responses to ATP and to CCE were significantly decreased (Figure 3F).

HCO_3^- Effect on Mitochondrial cAMP

The best-characterized activator of sAC is HCO_3^- (Steegborn et al., 2005b). The presence of 10 mM HCO_3^- in the medium increased both the number of ATP + TBHQ responsive cells (from 41% to 80%) and the size of their response (Figures 4A and 4B). The $\Delta R/R_0$ increase due to CCE, instead, was almost unaffected by the presence of 10 mM HCO_3^- in the medium (not shown). Figure 4C shows representative kinetics of $\Delta R/R_0$ changes in 4mtH30_E4 cells treated only with 50 mM $NaHCO_3$. The kinetic of the response to HCO_3^- was often biphasic, with an initial transient rise phase followed by a lower but sustained plateau (for over 30 min). The mean amplitude of the sustained plateau phase is summarized in Figure 4D. The response to HCO_3^- was significantly decreased in cells pretreated with the sAC inhibitor 2-hydroxy estradiol, 2-OHE (10 μM) (Figures 4C and 4D). The classical sAC inhibitor KH7, instead, caused a paradoxical dramatic increase of the mitochondrial $\Delta R/R_0$, but it was accompanied by a complete collapse of mitochondrial membrane potential (Figure S2) and ΔpH (not shown); accordingly, KH7 was not further tested. The overexpression of MCU had no effect on the cAMP response to HCO_3^- (not shown).

The interpretation of the effect of HCO_3^- and of the other treatments on cAMP using GFP-based probes is complicated by the possible influence of pH changes on the probe signal, as most GFP mutants are sensitive to pH changes in the physiological range (Abad et al., 2004; Llopis et al., 1998). To monitor the pH of the mitochondrial matrix, we transfected CHO cells with mtAlpHi, a genetically encoded mitochondrial pH indicator (Abad et al., 2004). The details of these experiments are presented in the Supplemental Information (Figure S3). We conclude that treatment with IBMX, EHNA (erythro-9-(2-hydroxy-3-nonyl)adenine), and 2-OHE had no appreciable effect on matrix pH, while a small and variable transient alkalinization was observed both upon ATP + TBHQ and CCE activation. Given that an alkalinization leads to an apparent decrease in cAMP, this effect of mitochondrial Ca^{2+} uptake on matrix pH tends, if anything, to slightly underestimate the $\Delta R/R_0$ increase. A significant transient acidification was observed upon addition of 50 mM

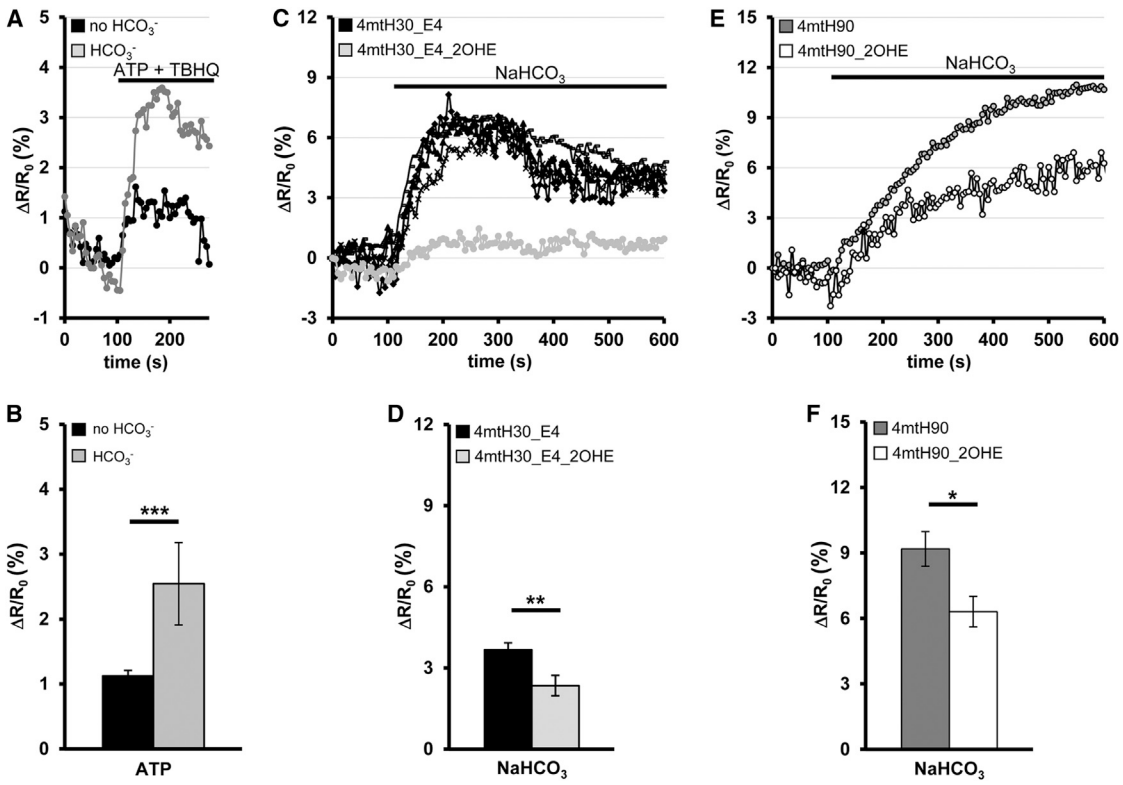

Figure 4. HCO_3^- Effect on Mitochondrial cAMP

(A) Representative kinetics of $\Delta R/R_0$ changes recorded in typical 4mtH30_E4 cells stimulated with ATP (50 μM) + TBHQ (30 μM), in the absence (black) or in the presence (gray) of 10 mM HCO_3^- in the medium.

(B) Average amplitude of the responses to ATP + TBHQ (mean ± SEM) in the absence or presence of HCO_3^- (n = 61 and n = 12, respectively; ***p = 7.3×10^{-5}).

(C) Representative kinetics of $\Delta R/R_0$ changes upon HCO_3^- addition (50 mM) in 4mtH30_E4 cells pretreated for 30 min with DMSO (black traces) or with the sAC inhibitor 2-hydroxy estradiol (2-OHE, 10 μM, gray trace).

(D) Average amplitude of the responses to HCO_3^- (mean ± SEM) (n = 71 controls, n = 31 2-OHE treated; **p = 0.0049).

(E) Representative kinetics of $\Delta R/R_0$ changes upon addition of HCO_3^- (50 mM) in CHO cells transiently expressing 4mtH90, pretreated for 30 min with DMSO (gray trace) or 2-OHE (10 μM, white trace).

(F) Average amplitude of the $\Delta R/R_0$ changes (mean ± SEM) caused by HCO_3^- (n = 23 and n = 21 for controls and 2-OHE treated, respectively; *p = 0.010). See also Figures S2 and S3.

$NaHCO_3$ (Figures S3E and S3F). We thus measured FRET changes in CHO cells transiently expressing a different cAMP sensor, 4mtH90 (kind gift of Dr. A. Hofer and Dr. K. Lefkimmiatis), much less pH sensitive than H30. Figure 4E shows typical kinetics of FRET changes in CHO cells expressing 4mtH90 and challenged with 50 mM HCO_3^-. The byphasic rise of $\Delta R/R_0$ was not observed, while the inhibitory effect of 2-OHE was maintained, as summarized in Figure 4F.

Mitochondrial cAMP Is Generated by sAC and Modulated by PDE

The above experiments and previous work (Acin-Perez et al., 2009) suggest that sAC is the enzyme responsible for the generation of cAMP in the mitochondrial matrix. To verify this conclusion, we performed genetic ablation of sAC by RNA silencing (see also Figure S4). The mt-cAMP increase caused by CCE activation was strongly reduced in silenced cells (Figure 5A), although the silencing of sAC had no effect on CCE (not shown). The CCE-dependent rise in mt-cAMP was inhibited, as in the case of HCO_3^-, by 2-OHE (Figure 5B), whereas it was unaffected by the carbonic anhydrase inhibitor acetazolamide (100 μM) and by the classical tmACs inhibitor 2′,3′-dideoxyadenosine (ddAdo, 100 μM) (not shown). Next, we tested the effect of overexpressing a mitochondria-targeted sAC. The 4mtH30_E4 cell line was cotransfected with a mitochondrial version of sAC (mt_trsAC) and with a cytosolic RFP, as a marker of transfection. Figure 5C summarizes the results on mt-cAMP induced by CCE activation in cells cotransfected with mt_trsAC and RFP. Overexpression of mt_trsAC markedly increased the Ca^{2+}-induced mt-cAMP production, and also in this case 2-OHE reduced the cAMP response to CCE (see Figure 5B). Finally, the absolute values of R, a function of the resting mt-cAMP levels, were slightly, but significantly, higher in unstimulated cells overexpressing mt_trsAC compared to untransfected controls (0.504 ± 0.007, n = 61 versus 0.486 ± 0.006, n = 97; p = 0.048).

In Figure 2 we showed that IBMX had a very small effect on resting mt-cAMP. In order to further address the role of PDEs, IBMX was added to cells whose cAMP was increased by either HCO_3^- or CCE. Figure 5D shows that IBMX caused in both cases a much larger mt-cAMP rise, and its effect was potentiated by overexpression of both MCU and mt_trsAC. It has been

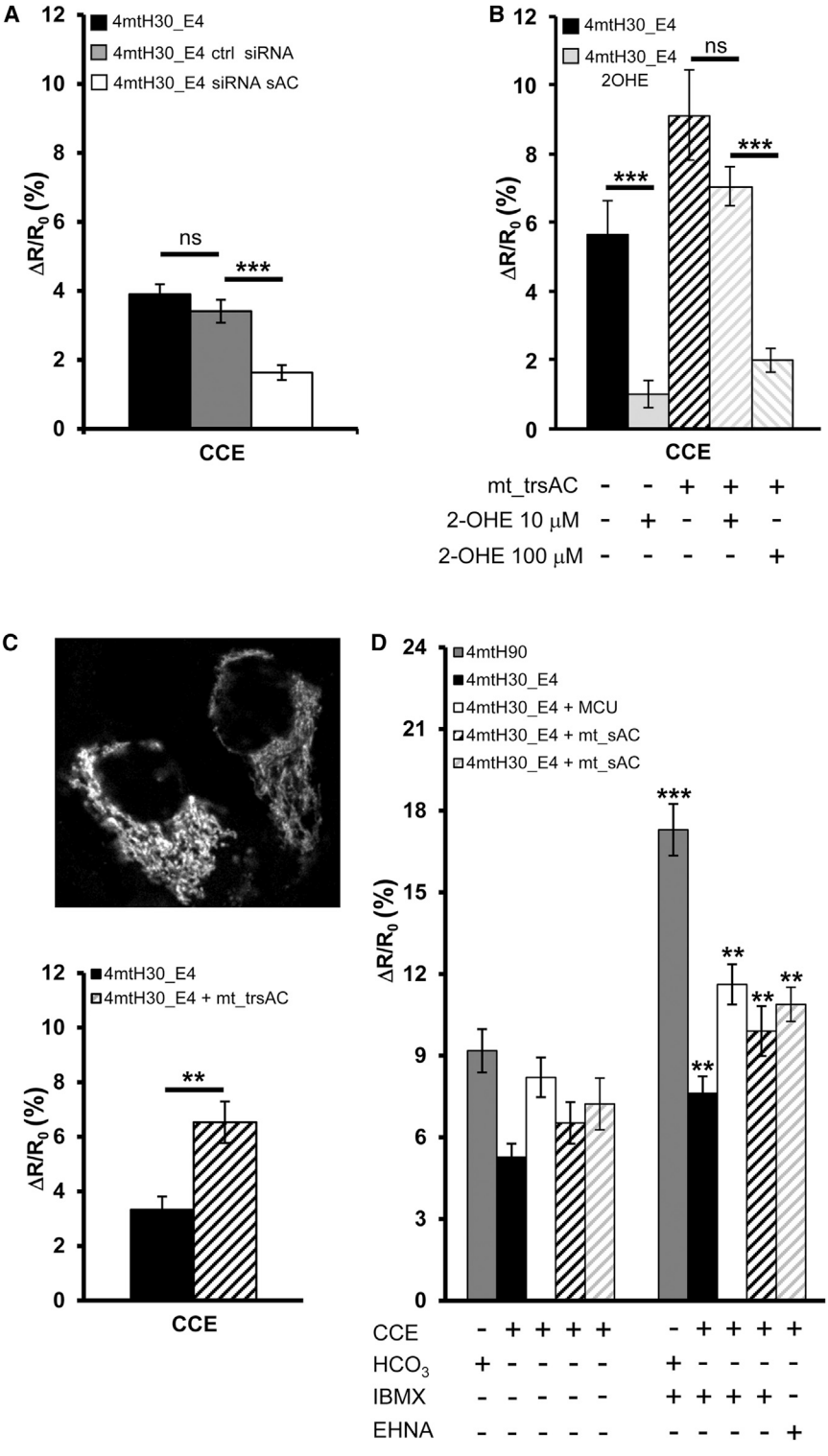

Figure 5. sAC and PDE Activities Modulate Mitochondrial cAMP

(A) Average (mean ± SEM) $\Delta R/R_0$ changes elicited by CCE (with the protocol described in Figure 3) in 4mtH30_E4 control cells (n = 72), in cells treated with the HMR1-MR2 siRNAs couple (n = 46), or with a control siRNA (n = 83) (p = 0.27 ctrl versus ctrl siRNA; ***p = 1.9×10^{-9} siRNA versus ctrl; ***p = 7.2×10^{-6} siRNA versus ctrl siRNA).

(B) Average (mean ± SEM) $\Delta R/R_0$ changes elicited by CCE in 4mtH30_E4 control cells pretreated for 30 min with DMSO (n = 11) or with 2-OHE, 10 μM (n = 70), ***p = 0.00018; average (mean ± SEM) $\Delta R/R_0$ changes elicited by CCE in 4mtH30_E4 cells cotransfected with a cytosolic RFP and mt_trsAC. Only cells coexpressing RFP were considered. Cells were treated for 30 min with DMSO (n = 15), with 2-OHE 10 μM (n = 24), or with 2-OHE 100 μM (n = 11). p = 0.11 for 2-OHE 10 μM versus controls and ***p = 0.0001 for 2-OHE 100 μM versus controls.

(C) Average (mean ± SEM) $\Delta R/R_0$ changes elicited by CCE in 4mtH30_E4 control cells (n = 19) and cells cotransfected with a cytosolic RFP and mt_trsAC (n = 43). Only cells coexpressing RFP were considered. **p = 0.0094. Inset: Confocal images of representatives CHO cells transfected with a RFP-tagged version of mt_trsAC.

(D) Average (mean ± SEM) $\Delta R/R_0$ changes elicited by the administration of IBMX (100 μM) on: 4mtH90-expressing cells previously stimulated with 50 mM $NaHCO_3$ (gray column; n = 23; ***p = 5.2×10^{-8} versus response to only $NaHCO_3$); 4mtH30_E4 cells previously subjected to CCE (black column; n = 26; **p = 0.0043 versus response only to CCE); 4mtH30_E4 cells overexpressing MCU and previously subjected to CCE (white column; n = 21; **p = 0.0021 versus response only to CCE); RFP-expressing 4mtH30_E4 cells transfected with RFP + mt_trsAC subjected to CCE (black-striped column; n = 43; **p = 0.0058 versus response only to CCE). The gray-striped column refers to the effect of the PDE2-selective inhibitor EHNA on RFP-expressing 4mtH30_E4 cells transfected with RFP + mt_trsAC previously subjected to CCE (n = 7; **p = 0.008 versus response only to CCE; p = 0.67 versus response to CCE/IBMX). See also Figures S3 and S4.

suggested that the PDE isoform in the mitochondrial matrix is PDE2A (Acin-Perez et al., 2011b). Indeed, administration of 10 μM EHNA, a PDE2-selective inhibitor, was almost as effective as IBMX at increasing the mt-cAMP rise in response to CCE (Figure 5D).

Functional Significance of Mitochondrial cAMP

Mitochondrial cAMP Modulates $[ATP]_m$

It has been proposed that a sAC-cAMP-PKA signaling pathway, wholly contained within mitochondria, modulates the respiratory chain enzymes through PKA-dependent phosphorylation (Acin-Perez et al., 2009, 2011a; Papa et al., 2008). We thus measured mitochondrial ATP concentration, $[ATP]_m$, in intact HeLa cells, making use of a matrix-targeted luciferase, mtLUC. Similar results were obtained in CHO cells. Figure 6 shows that the resting $[ATP]_m$ is increased ~40%

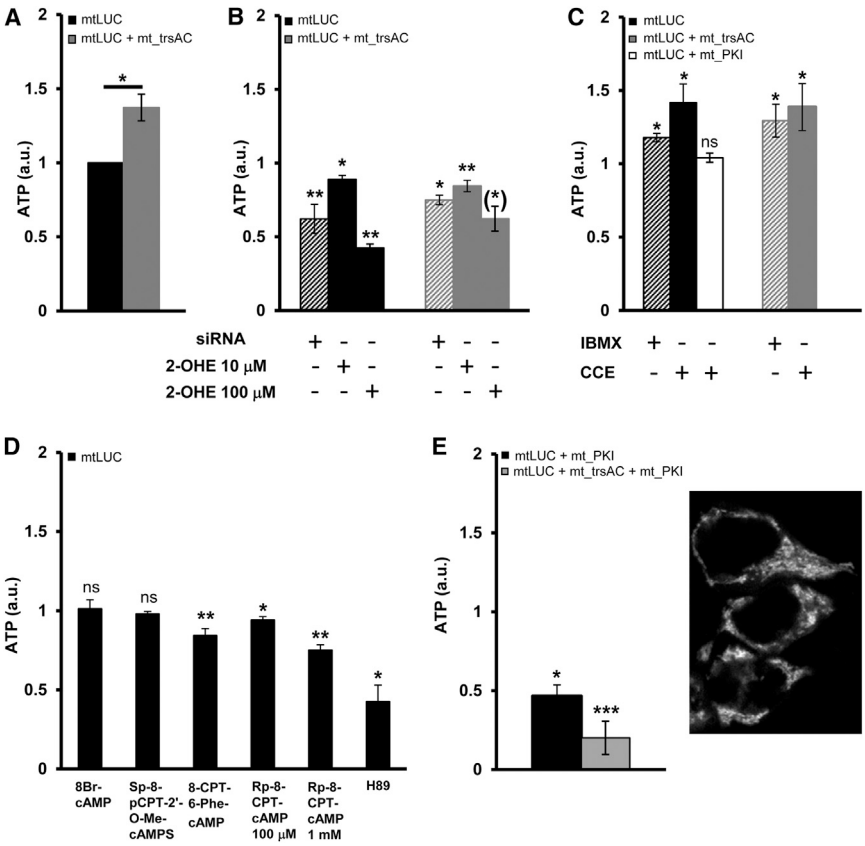

Figure 6. Effect of sAC Activity, mt-cAMP Increases, and PKA Inhibition/Activation on $[ATP]_m$

(A) Normalized (control = 1) average (mean ± SEM) $[ATP]_m$ basal levels measured in HeLa cells transfected with mtLUC alone or mtLUC + mt_trsAC. n = 34 experiments, *p = 0.025. In these and the following experiments, 30 min before measurement the medium was substituted with a HEPES-buffered Ringer-modified saline supplemented with luciferin (100 μM), and the cells were incubated at room temperature (20°C–22°C). Each condition was tested in triplicate in each experiment, and the means are derived from three or more independent experiments (as indicated). (A)–(E): two-tailed paired t tests.

(B) Normalized average (mean ± SEM) $[ATP]_m$ basal levels measured in cells cotransfected with mtLUC (black) or mtLUC + mt_trsAC (gray). Striped columns: The cells were incubated with HMR1-MR2 siRNAs against trsAC, and the basal luminescence measured was normalized to luminescence measured in cells incubated with control siRNA. Solid columns: the cells were treated with 2-OHE, 10 μM or 100 μM, for 2 hr before initiating the measurement, and the basal luminescence measured was normalized to luminescence measured in untreated controls. Other conditions as in (A). mtLUC_siRNA: n = 6, **p = 0.0071; mtLUC + mt_trsAC_siRNA: n = 3, *p = 0.022; mtLUC_2-OHE 10 μM: n = 4, *p = 0.036; mtLUC_2-OHE 100 μM: n = 6, **p = 0.0035; mtLUC + mt_trsAC_2-OHE 10 μM: n = 9, **p = 0.0096; mtLUC + mt_trsAC_2-OHE 100 μM: n = 4, *p = 0.051.

(C) Normalized average (mean ± SEM) $[ATP]_m$ measured in cells transfected with mtLUC alone (black), mtLUC + mt_PKI (white), or mtLUC + mt_trsAC (gray). Conditions as in (A). Striped columns: After initiating the $[ATP]_m$ measurement, the cells were treated with 100 μM IBMX for 15 min, and the final luminescence values have been normalized to their initial values. mtLUC: n = 6, *p = 0.013; mtLUC + mt_trsAC: n = 5, *p = 0.028. Solid columns: After initiating the $[ATP]_m$ measurement, CCE was initiated by addition of 2 mM $CaCl_2$ (see also Figure S5). For each sample, the final luminescence values 2 hr after Ca^{2+} addition have been normalized first to their initial values, then to values of untreated controls. In the case of mt_PKI, the transfection resulted in a reduction of the initial $[ATP]_m$ to about 45% of the control level (see E), and accordingly, the initial $[ATP]_m$ of the controls (cells transfected with mt_PKI and not subjected to CCE) has been set to 1; the CCE activation did not increase significantly this level. mtLUC: n = 3, *p = 0.013; mtLUC + mt_trsAC: n = 6, *p = 0.040; mtLUC + mt_PKI: n = 3, p = 0.33.

(D) Normalized average (mean ± SEM) $[ATP]_m$ measured in cells transfected with mtLUC. Conditions as in (A). After initiating the $[ATP]_m$ measurement, the cells were treated with several membrane-permeable cAMP analogs for 2 hr, and the final luminescence values were normalized to the initial values. The obtained values were then normalized to untreated controls. 8Br-cAMP (1 mM): n = 6, p = 0.94; Sp-8-pCPT-2′-O-Me-cAMPS (100 μM): n = 9, p = 0.18; 8-CPT-6-Phe-cAMP (100 μM): n = 10, **p = 0.0077; Rp-8-CPT-cAMP (100 μM and 1 mM): n = 9 and 3, respectively; *p = 0.038 and **p 0.0067, respectively; H89 (10 μM): n = 4, *p = 0.011.

(E) Normalized average (mean ± SEM) $[ATP]_m$ basal levels measured in cells transfected with mtLUC + mt_PKI (black) or with mtLUC + mt_trsAC + mt_PKI (gray). Conditions as in (A). The basal luminescence measured was normalized to luminescence measured in untransfected controls. mtLUC + mt_PKI: n = 7; *p = 0.035; mtLUC + mt_trsAC + mt_PKI: n = 22; ***p = 0.00011. Inset: confocal image of CHO cells transfected with a mCherry-tagged version of mt_PKI. See also Figures S5 and S6.

by mt_sAC cotransfection (Figure 6A), while specific siRNA for sAC reduced it both in mt_sAC-overexpressing and in control cells (Figure 6B). 2-OHE significantly reduced $[ATP]_m$, in a dose-dependent manner (Figure 6B), while IBMX increased it (Figure 6C). The effect on $[ATP]_m$ of CCE activation was then tested. Figure S5 shows typical changes in the kinetics of luciferase luminescence upon CCE activation, while in Figure 6C the average percentage increases are summarized. In both mtLUC and mtLUC + mt_trsAC transfected HeLa cells, both the rate and extent of $[ATP]_m$ increase were augmented upon CCE activation. The effect of CCE on $[ATP]_m$ was unaffected in the presence of the carbonic anhydrase inhibitor acetazolamide (100 μM, not shown).

Although the mechanism of PKA translocation into the mitochondrial matrix is still unknown, previous works suggest that the intramitochondrial effects of cAMP are mediated through the classical PKA pathway. We thus tested this hypothesis; to inhibit PKA, we treated the cells either with Rp-8-CPT-cAMP, a potent competitive inhibitor of cAMP binding to the PKA R subunit, or with H89 (5-isoquinolinesulfonamide) that competes for the ATP binding site of PKA C subunit. Both drugs clearly reduced $[ATP]_m$ (Figure 6D). Alternatively, we generated a mitochondrial targeted version of the endogenous protein kinase inhibitor peptide (PKI) (Figure 6E, inset). As shown in Figure 6E, mt_PKI overexpression reduced basal $[ATP]_m$ both in controls and in mt_trsAC-transfected cells. As the overexpression of mt_trsAC causes an increase of the basal $[ATP]_m$, in absolute terms the inhibition was comparable, reducing the basal $[ATP]_m$ of both control cells and mt_trsAC-overexpressing cells

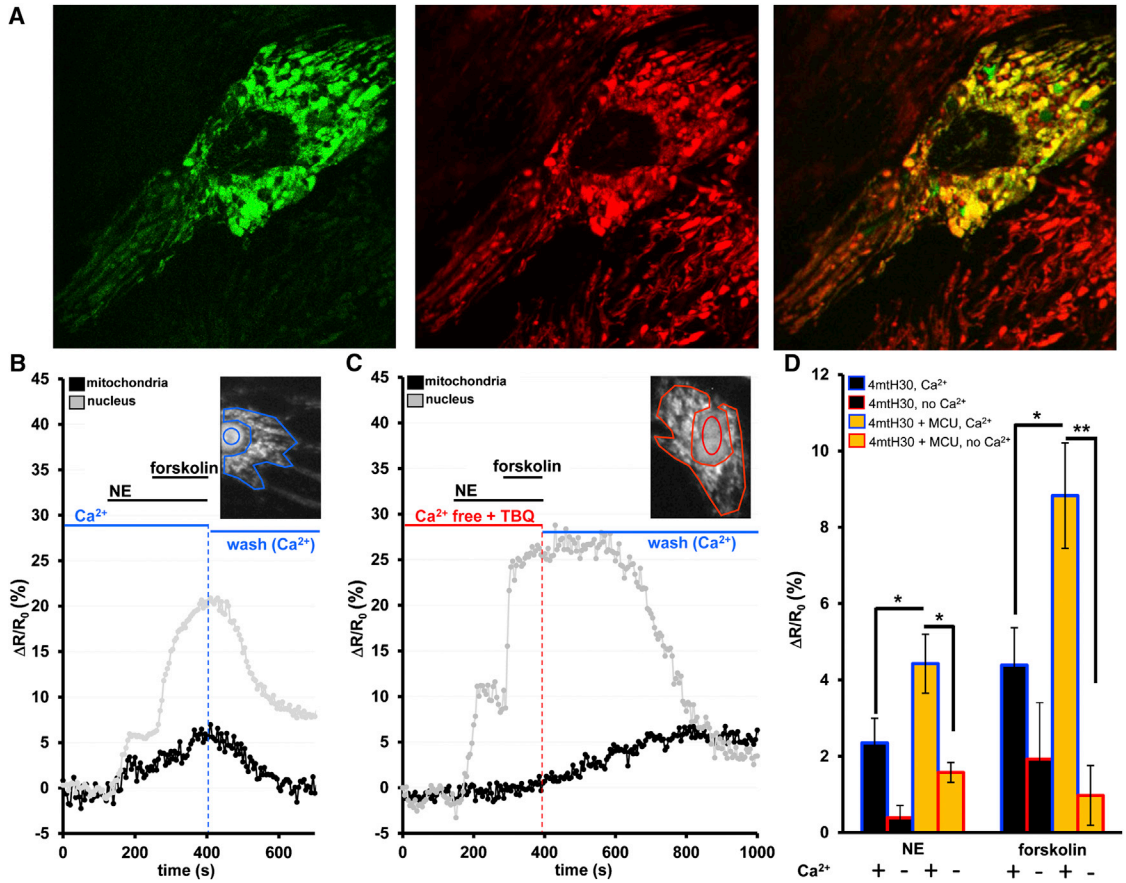

Figure 7. cAMP Is Elicited by Ca^{2+} Increases in the Mitochondrial Matrix of Neonatal Rat Cardiomyocytes

(A) Representative images of a primary cultured neonatal cardiomyocyte transfected with the cAMP sensor 4mtH30 (green) and stained with MitoTracker orange (red). The colocalization of 4mtH30 with MitoTracker orange is shown in yellow.

(B and C) Representative kinetics of $\Delta R/R_0$ changes recorded in a rat neonatal cardiomyocyte cotransfected with 4mtH30 and the nuclear cAMP sensor H30_NLS, stimulated, in sequence, with NE (10 μM) and forskolin (25 μM), in the presence (B) or in the absence (C) of $CaCl_2$ in the medium. The Ca^{2+}-free medium contained 100 μM EGTA and 30 μM TBQ.

(D) Average (mean ± SEM) $\Delta R/R_0$ changes recorded upon administration of NE (10 μM) and NE + forskolin (25 μM), in the presence or in the absence of $CaCl_2$ in the medium. $\Delta R/R_0$ changes have been recorded in the mitochondria of 4mtH30 (black columns; n = 9 in Ca^{2+} and n = 3 in Ca^{2+}-free; p = 0.11 for NE and p = 0.19 for forskolin) and 4mtH30 + MCU_mCherry-expressing cardiomyocytes (yellow columns; n = 7 in Ca^{2+} and n = 3 in Ca^{2+}-free; *p = 0.04 for NE and **p = 0.005 for forskolin). 4mtH30 versus 4mtH30 + MCU_mCherry: *p = 0.04 for NE and *p = 0.01 for forskolin. See also Figure S7.

to ~50% of the controls' basal $[ATP]_m$. Furthermore, in HeLa cells cotransfected with mtLUC and mt_PKI and subjected to CCE (Figure 6C), the rise of $[ATP]_m$ was strongly reduced by mt_PKI expression. We also tested Sp-8-pCPT-2′-O-Me-cAMPS (100 μM), the most permeable (~90 times more permeable than cAMP) of the Epac-selective cAMP analogs. Although this compound clearly penetrates the mitochondrial matrix (see Figure 1), it had no effect on $[ATP]_m$ (Figure 6D).

Taken as a whole, the above data appear consistent with the suggestion that the target of mt-cAMP is indeed PKA. As a final test, we investigated the effect on $[ATP]_m$ of two cAMP analogs, 8Br-cAMP (1 mM) and 8-CPT-6-Phe-cAMP (100 μM) (Figure 6D), that are known potent activators of cytosolic PKA, though they differ in terms of specificity and in permeability across membranes. Indeed, 8-CPT-6-Phe-cAMP is highly specific for PKA and 400-fold more permeable than cAMP while 8Br-cAMP activates other cAMP targets and is only twice as permeable as cAMP. Figure 6D shows that 8Br-cAMP had no effect on $[ATP]_m$, while 8-CPT-6-Phe-cAMP had a paradoxical effect, i.e., it decreased $[ATP]_m$. Yet 8Br-cAMP can reach the mitochondrial matrix and 8-CPT-6-Phe-cAMP is effective in activating cytosolic PKA (Figure S6).

Increased Frequency and Amplitude of Mitochondrial Ca^{2+} Oscillations Triggers Matrix cAMP Rises in Neonatal Rat Cardiomyocytes

Maximally stimulatory doses of an IP_3-generating agonist and activation of CCE in cell lines represent useful experimental tools to investigate the mechanism of cAMP control in mitochondria, but bear little relevance for the physiological significance of this pathway. To address the existence of a mitochondrial Ca^{2+}-cAMP crosstalk in a physiologically relevant model, we measured the cAMP dynamics in the mitochondrial matrix of primary cultured neonatal rat cardiomyocytes transfected with 4mtH30. Confocal analysis of a 4mtH30-expressing cardiomyocyte stained with MitoTracker is shown in Figure 7A. The sensor

distribution nicely overlapped that of the mitochondrial probe MitoTracker red, and only a very small missorting of the cAMP probe in the cytosol was observed in some cells. In order to follow in the same cells mitochondrial and cytosolic cAMP changes, we made use of the cotransfection with a nuclear version of the same sensor, H30_NLS (Terrin et al., 2006). The fluorescent signal of the sensors in the nucleus and mitochondria can be easily distinguished, and it has been shown previously that nuclear cAMP concentration closely follows the changes occurring in the cytoplasm. The cells, incubated either in Ca^{2+}-containing (Figure 7B) or Ca^{2+}-free medium (Figure 7C), were treated with 10 μM norepinephrine (NE), followed by 25 μM forskolin. The mitochondrial Ca^{2+} changes in these conditions are exemplified in Figure S7 (see also Robert et al., 2001). Figure 7B shows that, in the presence of 2 mM Ca^{2+}, both NE and forskolin evoke reversible cAMP increases, both inside and outside mitochondria; on the contrary (Figure 7C), when the same stimuli were applied in a Ca^{2+}-free medium, the cAMP increases in the nucleus were unaffected, whereas in the matrix they were drastically reduced. Under these latter conditions, removing the stimulus by perfusing with a Ca^{2+}-containing medium results in a rapid return of nuclear cAMP to basal level, while the mitochondrial level increased (Figure 7C). Most relevant, if the cells were also cotransfected with a mCherry-tagged version of the mitochondrial Ca^{2+} uniporter, MCU, which results in a substantial increase in the amplitude of mitochondrial Ca^{2+} accumulation (Drago et al., 2012), the mt-cAMP increases in response to both NE and forskolin were strongly potentiated in Ca^{2+}-containing medium; on the contrary, in the absence of Ca^{2+} the cAMP response was dramatically reduced. No significant difference in nuclear cAMP increases was observed depending on the presence/absence of Ca^{2+} in the medium (Figure S7).

DISCUSSION

For many years, the general consensus was that cAMP had no role within mitochondria, despite the existence of numerous potential PKA targets within this organelle (Technikova-Dobrova et al., 1994; Zhao et al., 2011). Among the most relevant arguments against a role of cAMP within mitochondria were: (1) cAMP is negatively charged and, due to the negative potential across the inner mitochondrial membrane, would tend to be excluded from the matrix; (2) no recognizable signal sequence is present either in the R or C PKA subunits; (3) all tmACs isoforms are localized at the plasma membrane. However, in the last years the existence of a soluble AC has been unraveled, and proteins recognized by antibodies against the PKA subunits have been found in the mitochondrial matrix (Schwoch et al., 1990). In addition, proteins such as AKAPs, Epac, PDEs, and sAC appear to be associated with mitochondria (Acin-Perez et al., 2009, 2011b; Breckler et al., 2011; Feliciello et al., 2001; Sardanelli et al., 2006). Finally, increasing evidence supports a key role of cAMP on the surface or in the matrix of the organelles (Acin-Perez et al., 2011a; Alto et al., 2002; Danial et al., 2003; Gomes et al., 2011; Harada et al., 1999; Sardanelli et al., 2006).

A key, yet unsolved, issue is whether cytosolic cAMP can enter the mitochondrial matrix. Unlike the results of DiPilato et al. (DiPilato et al., 2004), our data clearly demonstrate that even massive increases of cytosolic cAMP do not result in any significant change in mt-cAMP. Rather, our results indicate that mitochondria are endowed with an intrinsic sAC that is activated by a rise in matrix Ca^{2+} concentration and by HCO_3^-, while it is inhibited by blockers of sAC. We show that overexpression of a matrix-targeted sAC and sAC-silencing result in potentiation or inhibition, respectively, of the mt-cAMP increases elicited by HCO_3^-, IBMX, and CCE; moreover, the effect of Ca^{2+} and IBMX are potentiated by the presence of even low doses of HCO_3^-. A matrix-located PDE, inhibited by a specific PDE2 blocker, is responsible for local cAMP hydrolysis, as PDE inhibition causes in itself a very small increase in mt-cAMP of resting cells, and this effect is amplified when added on top of stimuli activating sAC. Of note, the Ca^{2+} responsible for the cAMP increase in the matrix is clearly that occurring within mitochondria and not the cytoplasmic one, as overexpression of MCU increases both mt-cAMP and Ca^{2+} levels, but reduces the cytosolic Ca^{2+} rises (De Stefani et al., 2011); in addition, silencing of MCU significantly decreases mt-cAMP. Importantly, we show that a matrix Ca^{2+} rise is a powerful stimulus to the generation of mt-cAMP in a physiologically relevant system as primary neonatal cardiomyocytes. Overall, these data clearly demonstrate that cAMP changes do occur in the mitochondrial matrix of living cells, independently from the cytosolic ones, and that these mitochondrial changes are due to the concerted action of intramitochondrial sAC and PDE. Most relevant, we show that a rise in matrix Ca^{2+} represents a potent stimulus for cAMP generation, in particular if it occurs in the presence of HCO_3^-.

Of particular relevance appear the results in cardiomyocytes stimulated with agents that, by activating tmACs, increase the level of cytosolic cAMP, thus augmenting frequency and amplitude of the spontaneous Ca^{2+} oscillations in the cytosolic and mitochondrial compartment (Robert et al., 2001). In this physiologically relevant model, the mitochondrial cAMP increases do not depend on the diffusion of the second messenger from the cytosol to the matrix, but rather from an endogenous cAMP production by the organelles, as in the cell lines model. This conclusion is based on the following evidence: (1) the rise of mt-cAMP is almost completely abolished by removal of extracellular Ca^{2+}, and (2) the mt-cAMP increase is augmented by increasing the amplitude of the mitochondrial Ca^{2+} uptake, as induced by MCU overexpression. Of note, the Ca^{2+} changes in the mitochondrial matrix are oscillatory, and each spike lasts 300–500 ms, while the organelle cAMP increases take a few tens of seconds to reach a new plateau level. Accordingly, this suggests that the intramitochondrial cAMP homeostatic machinery is capable of integrating an oscillatory Ca^{2+} signal in a prolonged cAMP increase.

The key final questions concern the functional consequences for mitochondrial metabolism of mt-cAMP changes and the identification of the enzyme(s) that decode the cAMP level within the organelle matrix. We show that the basal sAC activity modulates $[ATP]_m$, since increasing the mitochondrial sAC level results in a significant augmentation of mitochondrial ATP, while reducing its activity or level, with drugs or siRNA, decreases $[ATP]_m$. Furthermore, the rise in mt-cAMP, obtained by blocking PDEs or by activating CCE, increases $[ATP]_m$. The interpretation of the CCE effect on $[ATP]_m$ is, however, more complex, as the rise of matrix Ca^{2+} also activates the NADH-linked dehydrogenases, and this in itself may be sufficient to increase respiration

and ATP production (Jouaville et al., 1999; Wiederkehr et al., 2011). Moreover, ATP itself has an inhibitory effect on sAC (Litvin et al., 2003), and this substrate inhibition is relieved as the bicarbonate concentration increases. Therefore, Ca^{2+} could have a further, indirect, effect on sAC, inasmuch as the dehydrogenase activation increases respiration, and thus HCO_3^- concentration, and this could, through relieving the ATP inhibition, contribute to a further sAC activation. We can speculate that the effects of Ca^{2+} on the dehydrogenases and cAMP levels synergize to insure an optimal flux of electrons in the respiratory chain and an appropriate rate of ATP synthesis in stimulated cells.

As to the target of mt-cAMP, the most obvious candidate is PKA. Indeed, evidence has been provided for the existence of PKA within mitochondria (Sardanelli et al., 2006; Schwoch et al., 1990; Acin-Perez et al., 2009), and we here show that the effects of different agents on $[ATP]_m$ are inhibited not only by the classical PKA inhibitor H89 (though its specificity is low) or by Rp-8-CPT-cAMP, which competes with the cAMP binding site of R-subunit, but also by a mitochondrial targeted PKI, considered the most specific endogenous PKA inhibitor. We can exclude that the effects on ATP are somehow mediated through cytosolic cAMP, as neither 8Br-cAMP nor 8-CPT-6-Phe-cAMP, potent activators of cytosolic PKA, increase $[ATP]_m$. On the contrary, 8-CPT-6-Phe-cAMP, which is considered the most specific activator of PKA, rather than stimulating ATP production results in a modest reduction of ATP level. These last unexpected pharmacological properties require further investigation and suggest that the enzyme trapped in the mitochondrial matrix may possess unique properties compared to canonical cytosolic PKA.

EXPERIMENTAL PROCEDURES

Fluorescence Resonance Energy Transfer Imaging

FRET imaging experiments were performed 24–48 hr after cell transfection or in the stable line. Cells were maintained at room temperature (20°C–22°C) in HEPES-buffered Ringer-modified saline (see Supplemental Information) supplemented with $CaCl_2$ (2 mM) or, alternatively, EGTA 100 μM (Ca^{2+}-free conditions) and imaged with an inverted microscope (Olympus IX50) equipped with a CellR imaging system and a beam-splitter optical device (Multispec Microimager; Optical Insights). Images were acquired every 5 s (10 s during the TMRM experiments) with a 60×, 1.4 NA oil-immersion objective (Olympus) using the CellR software and processed using ImageJ (http://rsb.info.nih.gov/ij/). FRET changes were measured as changes in the background-subtracted 480/545 nm fluorescence emission intensities upon excitation at 430 nm and expressed as $\Delta R/R_0$, where R is the ratio at time t and R_0 is the ratio at time = 0 s; $\Delta R = R - R_0$.

Confocal Imaging

Confocal images were acquired 24–48 hr after transfection or in the stable cell line by using the broadband confocal Leica TCS SP5 system (Leica Microsystems) and a HCX PL APO 63×, 1.4 NA oil-immersion objective. Cells were maintained in HEPES-buffered Ringer-modified saline (see Supplemental Information) supplemented with 2 mM $CaCl_2$, at room temperature (20°C–22°C), and excited using the 458 nm line of an argon laser for imaging CFP and the 543 nm line of a helium-neon laser for imaging mRFP.

ATP Measurements

To measure mitochondrial ATP levels, HeLa cells grown on 24-well plates at 60%–70% confluence were transfected with mitochondria-targeted luciferase (mtLUC) or cotransfected with mtLUC and other cDNAs and/or treated with the siRNAs. At 24–48 hr after transfection, luminescence experiments were carried out. Thirty minutes before measurement, the medium was substituted with a HEPES-buffered Ringer-modified saline (identical to that used in FRET CCE experiments), without $CaCl_2$ and supplemented with 100 μM EGTA and 100 μM luciferin, and cells were incubated at room temperature (20°C–22°C). Luminescence was measured at room temperature with a FLUOstar OPTIMA (BMG Labtechologies, Inc.), acquiring the luminescence value from each well every minute, in plate mode. A baseline was established in 15–20 cycles, each consisting of a full plate reading of the luminescence values. Cells were then treated with the different reagents, as indicated. Values recorded from wells containing untransfected cells were used as background, and subtracted from the values of transfected cells.

Statistical Tests

In each graph, unless noted, data represent mean ± SEM of the indicated number (n) of independent experiments. Statistical significance has been calculated by a two-tailed Student's t test (or, when indicated, by a two-tailed Student's paired t test). P values are indicated in the figure legends.

SUPPLEMENTAL INFORMATION

Supplemental Information includes seven figures and Supplemental Experimental Procedures and can be found with this article online at http://dx.doi.org/10.1016/j.cmet.2013.05.003.

ACKNOWLEDGMENTS

This research was supported by grants from the Italian Institute of Technology (IIT, Seed Project), the Italian Ministry of Education (PRIN 2009CCZSES_002 and FIRB RBAP11X42L projects), the CARIPARO Foundation (mitochondrial Ca^{2+} uptake and cardiac pathophysiology), and the Veneto Region (RISIB project) to T.P. and from the European Community's Seventh Framework Program FP7/2007-2013 under grant agreement no HEALTH-F2-2009-241526, EUTrigTreat, to M.M. We thank A. Hofer, K. Lefkimmiatis, and M. Conti for cDNA constructs and helpful discussions; A. Raffaello, D. De Stefani, and R. Rizzuto, for cDNA constructs and for siRNAs; and P.J. Magalhães for critically reading the manuscript.

Received: November 21, 2012
Revised: March 8, 2013
Accepted: April 8, 2013
Published: June 4, 2013

REFERENCES

Abad, M.F., Di Benedetto, G., Magalhães, P.J., Filippin, L., and Pozzan, T. (2004). Mitochondrial pH monitored by a new engineered green fluorescent protein mutant. J. Biol. Chem. *279*, 11521–11529.

Acin-Perez, R., Salazar, E., Kamenetsky, M., Buck, J., Levin, L.R., and Manfredi, G. (2009). Cyclic AMP produced inside mitochondria regulates oxidative phosphorylation. Cell Metab. *9*, 265–276.

Acin-Perez, R., Gatti, D.L., Bai, Y., and Manfredi, G. (2011a). Protein phosphorylation and prevention of cytochrome oxidase inhibition by ATP: coupled mechanisms of energy metabolism regulation. Cell Metab. *13*, 712–719.

Acin-Perez, R., Russwurm, M., Günnewig, K., Gertz, M., Zoidl, G., Ramos, L., Buck, J., Levin, L.R., Rassow, J., Manfredi, G., and Steegborn, C. (2011b). A phosphodiesterase 2A isoform localized to mitochondria regulates respiration. J. Biol. Chem. *286*, 30423–30432.

Alto, N.M., Soderling, J., and Scott, J.D. (2002). Rab32 is an A-kinase anchoring protein and participates in mitochondrial dynamics. J. Cell Biol. *158*, 659–668.

Balaban, R.S. (2010). The mitochondrial proteome: a dynamic functional program in tissues and disease states. Environ. Mol. Mutagen. *51*, 352–359.

Baughman, J.M., Perocchi, F., Girgis, H.S., Plovanich, M., Belcher-Timme, C.A., Sancak, Y., Bao, X.R., Strittmatter, L., Goldberger, O., Bogorad, R.L., et al. (2011). Integrative genomics identifies MCU as an essential component of the mitochondrial calcium uniporter. Nature *476*, 341–345.

Boja, E.S., Phillips, D., French, S.A., Harris, R.A., and Balaban, R.S. (2009). Quantitative mitochondrial phosphoproteomics using iTRAQ on an LTQ-Orbitrap with high energy collision dissociation. J. Proteome Res. *8*, 4665–4675.

Breckler, M., Berthouze, M., Laurent, A.C., Crozatier, B., Morel, E., and Lezoualc'h, F. (2011). Rap-linked cAMP signaling Epac proteins: compartmentation, functioning and disease implications. Cell. Signal. *23*, 1257–1266.

Carlucci, A., Adornetto, A., Scorziello, A., Viggiano, D., Foca, M., Cuomo, O., Annunziato, L., Gottesman, M., and Feliciello, A. (2008). Proteolysis of AKAP121 regulates mitochondrial activity during cellular hypoxia and brain ischaemia. EMBO J. *27*, 1073–1084.

Chen, Q., Lin, R.Y., and Rubin, C.S. (1997). Organelle-specific targeting of protein kinase AII (PKAII). Molecular and in situ characterization of murine A kinase anchor proteins that recruit regulatory subunits of PKAII to the cytoplasmic surface of mitochondria. J. Biol. Chem. *272*, 15247–15257.

Chen, Y., Cann, M.J., Litvin, T.N., Iourgenko, V., Sinclair, M.L., Levin, L.R., and Buck, J. (2000). Soluble adenylyl cyclase as an evolutionarily conserved bicarbonate sensor. Science *289*, 625–628.

Danial, N.N., Gramm, C.F., Scorrano, L., Zhang, C.Y., Krauss, S., Ranger, A.M., Datta, S.R., Greenberg, M.E., Licklider, L.J., Lowell, B.B., et al. (2003). BAD and glucokinase reside in a mitochondrial complex that integrates glycolysis and apoptosis. Nature *424*, 952–956.

De Stefani, D., Raffaello, A., Teardo, E., Szabò, I., and Rizzuto, R. (2011). A forty-kilodalton protein of the inner membrane is the mitochondrial calcium uniporter. Nature *476*, 336–340.

DiPilato, L.M., Cheng, X., and Zhang, J. (2004). Fluorescent indicators of cAMP and Epac activation reveal differential dynamics of cAMP signaling within discrete subcellular compartments. Proc. Natl. Acad. Sci. USA *101*, 16513–16518.

Drago, I., De Stefani, D., Rizzuto, R., and Pozzan, T. (2012). Mitochondrial Ca2+ uptake contributes to buffering cytoplasmic Ca2+ peaks in cardiomyocytes. Proc. Natl. Acad. Sci. USA *109*, 12986–12991.

Feliciello, A., Gottesman, M.E., and Avvedimento, E.V. (2001). The biological functions of A-kinase anchor proteins. J. Mol. Biol. *308*, 99–114.

Filippin, L., Abad, M.C., Gastaldello, S., Magalhães, P.J., Sandonà, D., and Pozzan, T. (2005). Improved strategies for the delivery of GFP-based Ca^{2+} sensors into the mitochondrial matrix. Cell Calcium *37*, 129–136.

Giacomello, M., Drago, I., Bortolozzi, M., Scorzeto, M., Gianelle, A., Pizzo, P., and Pozzan, T. (2010). Ca^{2+} hot spots on the mitochondrial surface are generated by Ca^{2+} mobilization from stores, but not by activation of store-operated Ca^{2+} channels. Mol. Cell *38*, 280–290.

Gomes, L.C., Di Benedetto, G., and Scorrano, L. (2011). During autophagy mitochondria elongate, are spared from degradation and sustain cell viability. Nat. Cell Biol. *13*, 589–598.

Harada, H., Becknell, B., Wilm, M., Mann, M., Huang, L.J., Taylor, S.S., Scott, J.D., and Korsmeyer, S.J. (1999). Phosphorylation and inactivation of BAD by mitochondria-anchored protein kinase A. Mol. Cell *3*, 413–422.

Hopper, R.K., Carroll, S., Aponte, A.M., Johnson, D.T., French, S., Shen, R.-F., Witzmann, F.A., Harris, R.A., and Balaban, R.S. (2006). Mitochondrial matrix phosphoproteome: effect of extra mitochondrial calcium. Biochemistry *45*, 2524–2536.

Huang, L.J., Wang, L., Ma, Y., Durick, K., Perkins, G., Deerinck, T.J., Ellisman, M.H., and Taylor, S.S. (1999). NH2-Terminal targeting motifs direct dual specificity A-kinase-anchoring protein 1 (D-AKAP1) to either mitochondria or endoplasmic reticulum. J. Cell Biol. *145*, 951–959.

Jaiswal, B.S., and Conti, M. (2003). Calcium regulation of the soluble adenylyl cyclase expressed in mammalian spermatozoa. Proc. Natl. Acad. Sci. USA *100*, 10676–10681.

Jouaville, L.S., Pinton, P., Bastianutto, C., Rutter, G.A., and Rizzuto, R. (1999). Regulation of mitochondrial ATP synthesis by calcium: evidence for a long-term metabolic priming. Proc. Natl. Acad. Sci. USA *96*, 13807–13812.

Litvin, T.N., Kamenetsky, M., Zarifyan, A., Buck, J., and Levin, L.R. (2003). Kinetic properties of "soluble" adenylyl cyclase. Synergism between calcium and bicarbonate. J. Biol. Chem. *278*, 15922–15926.

Liu, J., Li, H., and Papadopoulos, V. (2003). PAP7, a PBR/PKA-RIalpha-associated protein: a new element in the relay of the hormonal induction of steroidogenesis. J. Steroid Biochem. Mol. Biol. *85*, 275–283.

Llopis, J., McCaffery, J.M., Miyawaki, A., Farquhar, M.G., and Tsien, R.Y. (1998). Measurement of cytosolic, mitochondrial, and Golgi pH in single living cells with green fluorescent proteins. Proc. Natl. Acad. Sci. USA *95*, 6803–6808.

Means, C.K., Lygren, B., Langeberg, L.K., Jain, A., Dixon, R.E., Vega, A.L., Gold, M.G., Petrosyan, S., Taylor, S.S., Murphy, A.N., et al. (2011). An entirely specific type I A-kinase anchoring protein that can sequester two molecules of protein kinase A at mitochondria. Proc. Natl. Acad. Sci. USA *108*, E1227–E1235.

Nikolaev, V.O., Bünemann, M., Hein, L., Hannawacker, A., and Lohse, M.J. (2004). Novel single chain cAMP sensors for receptor-induced signal propagation. J. Biol. Chem. *279*, 37215–37218.

Papa, S., De Rasmo, D., Scacco, S., Signorile, A., Technikova-Dobrova, Z., Palmisano, G., Sardanelli, A.M., Papa, F., Panelli, D., Scaringi, R., and Santeramo, A. (2008). Mammalian complex I: a regulable and vulnerable pacemaker in mitochondrial respiratory function. Biochim. Biophys. Acta *1777*, 719–728.

Parekh, A.B., and Putney, J.W., Jr. (2005). Store-operated calcium channels. Physiol. Rev. *85*, 757–810.

Ponsioen, B., Zhao, J., Riedl, J., Zwartkruis, F., van der Krogt, G., Zaccolo, M., Moolenaar, W.H., Bos, J.L., and Jalink, K. (2004). Detecting cAMP-induced Epac activation by fluorescence resonance energy transfer: Epac as a novel cAMP indicator. EMBO Rep. *5*, 1176–1180.

Putney, J.W. (2009). Capacitative calcium entry: from concept to molecules. Immunol. Rev. *231*, 10–22.

Robert, V., Gurlini, P., Tosello, V., Nagai, T., Miyawaki, A., Di Lisa, F., and Pozzan, T. (2001). Beat-to-beat oscillations of mitochondrial [Ca^{2+}] in cardiac cells. EMBO J. *20*, 4998–5007.

Sardanelli, A.M., Signorile, A., Nuzzi, R., Rasmo, D.D., Technikova-Dobrova, Z., Drahota, Z., Occhiello, A., Pica, A., and Papa, S. (2006). Occurrence of A-kinase anchor protein and associated cAMP-dependent protein kinase in the inner compartment of mammalian mitochondria. FEBS Lett. *580*, 5690–5696.

Schwoch, G., Trinczek, B., and Bode, C. (1990). Localization of catalytic and regulatory subunits of cyclic AMP-dependent protein kinases in mitochondria from various rat tissues. Biochem. J. *270*, 181–188.

Steegborn, C., Litvin, T.N., Hess, K.C., Capper, A.B., Taussig, R., Buck, J., Levin, L.R., and Wu, H. (2005a). A novel mechanism for adenylyl cyclase inhibition from the crystal structure of its complex with catechol estrogen. J. Biol. Chem. *280*, 31754–31759.

Steegborn, C., Litvin, T.N., Levin, L.R., Buck, J., and Wu, H. (2005b). Bicarbonate activation of adenylyl cyclase via promotion of catalytic active site closure and metal recruitment. Nat. Struct. Mol. Biol. *12*, 32–37.

Technikova-Dobrova, Z., Sardanelli, A.M., Stanca, M.R., and Papa, S. (1994). cAMP-dependent protein phosphorylation in mitochondria of bovine heart. FEBS Lett. *350*, 187–191.

Terrin, A., Di Benedetto, G., Pertegato, V., Cheung, Y.F., Baillie, G., Lynch, M.J., Elvassore, N., Prinz, A., Herberg, F.W., Houslay, M.D., and Zaccolo, M. (2006). PGE(1) stimulation of HEK293 cells generates multiple contiguous domains with different [cAMP]: role of compartmentalized phosphodiesterases. J. Cell Biol. *175*, 441–451.

Wiederkehr, A., Szanda, G., Akhmedov, D., Mataki, C., Heizmann, C.W., Schoonjans, K., Pozzan, T., Spät, A., and Wollheim, C.B. (2011). Mitochondrial matrix calcium is an activating signal for hormone secretion. Cell Metab. *13*, 601–611.

Zhao, X., León, I.R., Bak, S., Mogensen, M., Wrzesinski, K., Højlund, K., and Jensen, O.N. (2011). Phosphoproteome analysis of functional mitochondria isolated from resting human muscle reveals extensive phosphorylation of inner membrane protein complexes and enzymes. Mol. Cell. Proteomics *10*, M110, 000299.